Journal of the Hellenic Veterinary Medical Society

Vol 75, No 3 (2024)

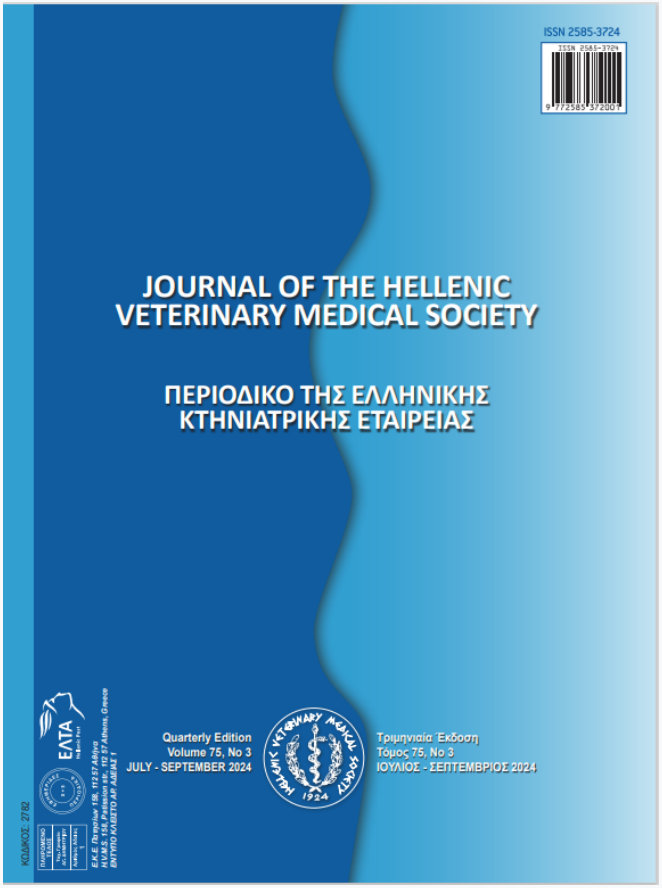

Morphological characteristics of rabbits' carpal tunnel: Evaluation of its potential for carpal tunnel research

F Turker Yavas, I Dabanoglu

doi: 10.12681/jhvms.37030

To cite this article:

Turker Yavas, F., & Dabanoglu, I. (2024). Morphological characteristics of rabbits' carpal tunnel: Evaluation of its potential for carpal tunnel research. *Journal of the Hellenic Veterinary Medical Society*, *75*(3), 8073–8082. https://doi.org/10.12681/jhvms.37030

J HELLENIC VET MED SOC 2024, 75 (3): 8073-8082
ΠΕΚΕ 2024, 75 (3): 8073-8082

Research article
Ερευνητικό άρθρο

Morphological characteristics of rabbits' carpal tunnel: Evaluation of its potential for carpal tunnel research

F. Turker Yavas, I. Dabanoglu

Department of Anatomy, Faculty of Veterinary Medicine, Aydin Adnan Menderes University, Aydin, Turkey

ABSTRACT: This study aimed to define the main anatomic components and describe the normal size and form of the carpal tunnel in rabbits using imaging techniques. It was also aimed to evaluate the potential of rabbits as an animal model for carpal tunnel research. The forelimbs of eight adult New Zealand rabbits were investigated using histology, magnetic resonance, and computed tomography. Two cadavers were used for anatomical dissection to support the findings. The carpal tunnel was examined at proximal and distal levels, and it was found that the flexor retinaculum is two-layered in rabbits. Both vascular nerve bundles, including the median nerve and the ramus palmaris of the ulnar nerve, were within two layers of it and passed through the carpal tunnel. The deep digital flexor, superficial digital flexor, and radial carpal flexor tendons were observed within the carpal tunnel. The flexor pollicis longus tendon is not found in rabbits. The area of the carpal tunnel narrowed towards the distal end in three methods, and its depth decreased in CT and MRI. The length of the accessory carpal bone determined this depth. The study found that rabbits' carpal tunnels are morphologically similar to those of humans compared to dogs. This situation is thought to pave the way for more accurate approaches to carpal tunnel research in rabbits.

***Keywords*:** Carpal canal; computed tomography; histology; magnetic resonance; morphometry.

Corresponding Author:
Ilknur Dabanoglu, Aydin Adnan Menderes University, Faculty of Veterinary Medicine, Department of Anatomy, Isikli, 09020, Efeler/ Aydin, Turkey.
E-mail address: idabanoglu@adu.edu.tr

Date of initial submission: 21-02-2024
Date of acceptance: 08-03-2024

INTRODUCTION

The carpal tunnel is an osteofibrous canal located along the wrist's palmar aspect, containing flexor tendons, the median nerve, the median artery, and the median vein (Craige, 1948; Ettema *et al.* 2006; Schrier *et al.,* 2020). The proximal row of carpal bones, particularly the accessory carpal bone, which provides the formation of the groove, forms the entrance of the carpal tunnel in humans. The exit of it is formed by the distal row of carpal bones; especially the hook of the hamate bone (Sora and Genser-Strobl, 2005; Preazzi *et al*. 2011; Park *et al.* 2020). In dogs, the carpal tunnel is shaped only by the accessory carpal bone, since the hamate does not have a hook. The entrance has been assessed at the level of the distal radio-ulnar joint and the palmar protrusion of the accessory carpal bone. The exit has been evaluated at the level of the proximal row of carpal bones, including the accessory carpal bone (Turan and Eren, 2003).

It is crucial for carpal tunnel syndrome (CTS), a common entrapment neuropathy in humans caused by compression of the median nerve (Diao *et al.,* 2005; Bower *et al.,* 2006). The condition can be costly, with treatment costing over $2 billion annually in the USA and $13,200 per person in Canada (Kamolz *et al.,* 2001; Stapleton, 2006; Wright and Atkinson, 2019; Zoniga and Keir, 2019). To diagnose and examine the anatomical structure of carpal tunnel, imaging techniques like CT (Computed Tomography) and MR (Magnetic Resonance) are used (Oh et al. 2008; Deruddere et al., 2014). Experimental animal studies, particularly rabbits, have been preferred due to their similarity to humans (Ettema *et al.,* 2006; Schrier *et al.,* 2020), easy availability, cheap feeding, and practical care conditions (Diao *et al.,* 2005; Oh *et al.* 2008; Yamaguchi *et al.,* 2008; Tung *et al.,* 2010; Moriya *et al.,* 2011; Yoshii *et al.,* 2014).

However, these investigations often contain insufficient and inaccurate anatomical information, and there is no study on the detailed morphological and morphometric structure of the carpal tunnel in rabbits. This study aims to describe the anatomical structures and normal shape and size of the carpal tunnel in rabbits using CT, MRI, and histological methods and to reveal possible differences by comparing the images obtained with these methods.

MATERIALS AND METHODS

Ethical statement

The study was approved by Aydın Adnan Menderes University Local Ethics committee (Decision number: 645583101/2017/141 and 64583101/2022/008).

Animal material

This study used eight adult New Zealand rabbits (*Oryctolagus cuniculus L*.) frozen in 10 % formalin. Rabbits averaged 2.137 grams. After MRI and CT scans, cadavers were histologically sectioned. Additionally, two rabbits were dissected for anatomy.

Computed Tomography (CT)

An 80 detector 160 slice computed tomography (CT) System (Aquilion Prime, Toshiba Medical Systems, Otawara, Japan) was used. The rabbits' prone forelimbs were scanned. 1 mm thick pictures were taken. CT images were made at 120 kV and 200 mAs. The FOV is 140 mm. CT measurements were taken with Sectra IDS7, which is the Adnan Menderes University pacs system. This system is a picture archive and communication system.

Magnetic Resonance Imaging (MRI)

A Philips 3 Tesla Dstream Achieva Digital MR (made in the south of the Netherlands) was used. The small digital channel coil was taken to see the rabbits' wrists in the prone position. T1 and T2 were mostly scanned at 1 mm. T1-weighted pictures have 7.1 ms TR, 3.4 ms TE, 244 x 240 matrix, and 170 mm FOV; T2-weighted images have 1300 ms TR, 186 ms TE, and 192 x 155 matrix. The Mediapacs Viewer program was used to take measurements on MR images obtained from a private imaging center.

Histological Section (HS)

Carpal tissue was preserved in 10% buffered formalin and decalcified in 10% nitric acid. It was trimmed after sufficient decalcification for around 5 days. After multiple treatments with xylol and increasing alcohol solutions (70°, 80°, 90°, 96°, and 100°), the tissues were taken to the Leica TP1020 tissue tracking device and blocked in paraffin. These blocks were microtome-cut and stained with hematoxylin and eosin (H&E) (Luna, 1968). The digital images taken using an Olympus SZX-LGR66 stereomicroscope were stored. Histological slices were photographed with a stereomicroscope and measurement paper. After transferring the photos to BSD-2-licensed ImageJ, measurements were taken.

Measurements

The measurements of the carpal canal and identi-

fication of the anatomical structures were carried out at two levels. The proximal level was defined as the entrance to the carpal tunnel at the ends of the radius and ulna, where the palmar projection of the accessory carpal bone could be seen. The distal level was defined as the carpal tunnel and included the proximal row of the carpal bones. The measurements taken are listed below.

Total carpal area (TCA); The area of the carpal region that includes all the anatomical structures under the skin (Figure 1).

Carpal tunnel area (CTA); At the two levels, the carpal tunnel area was measured between the flexor retinaculum and the bones (Figure 1 &2).

Bone area (BA); The area was measured by aligning the borders of the bones at both the proximal and distal levels (Figure 1 & 2).

Carpal tunnel width (CTW); At the proximal level, the transverse distance between the radius's styloid process and the accessory carpal bone's medial palmar process was measured. At the distal level, the transversal distance was measured between the medial palmar process of the accessory carpal bone and the palmomedial process of the radial carpal bone (Figure 1 & 2).

Carpal tunnel depth (CTD); The vertical distance between the deepest palmar border of the bones and the flexor retinaculum was measured at both levels (Figure 1 & 2).

Accessory carpal bone length (CAL); It was measured at the distal level. For this, a line was drawn connecting the two dorsal projections of this bone. The vertical distance was measured between the midpoint of this line and the palmar top of the bone.

Statistical Evaluation

SPSS Statistics 21.0 analysed the data. For dependent variables, the paired t-test was employed for parametric data and the Wilcoxon test for nonparametric data to compare carpal tunnel techniques and interregional measurements. The tables provide Mean ± Standard deviation (Mean±Std). All calculations had a statistically significant P-value below 0.05.

RESULTS

The anatomical structures and the normal shape and size of the carpal tunnel in rabbits were defined

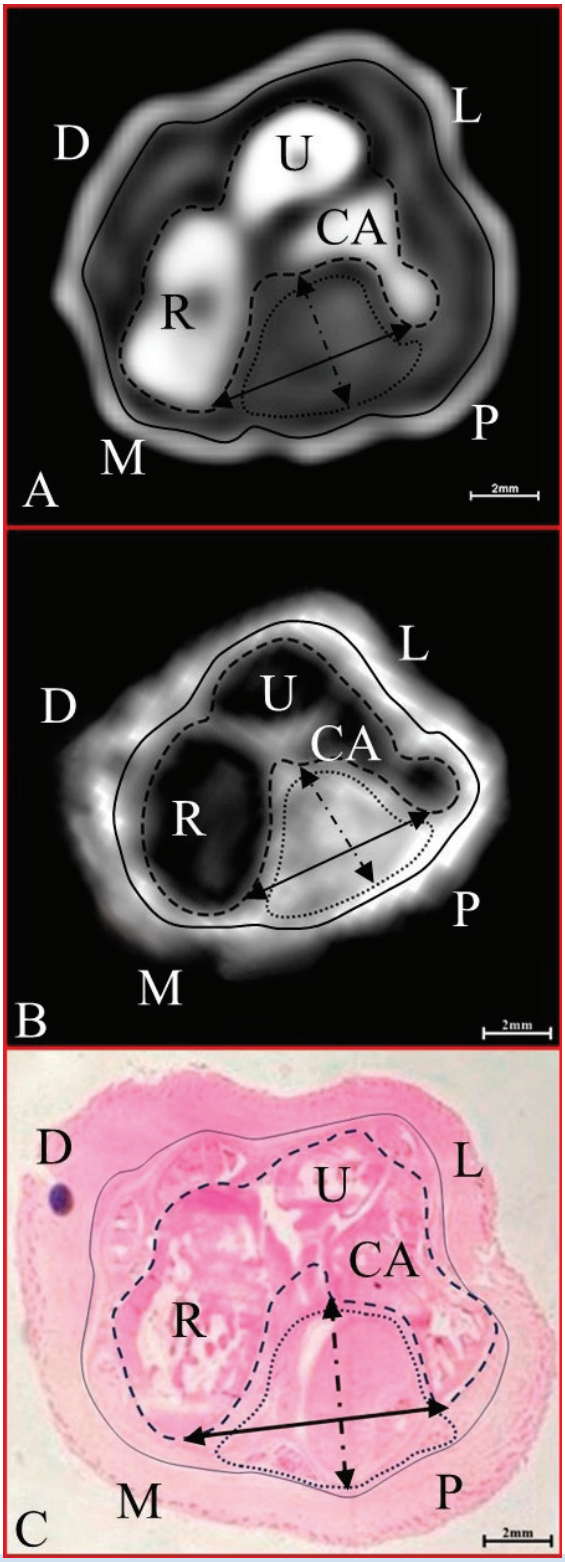

Figure 1. Images from computed tomography (bony window) (A), magnetic resonance (T1W) (B) and histological section (C) (H&E, 2X magnification) at the proximal level. R; radius, U; ulna, CA; accessory carpal bone, M; medial side, L; lateral side, D; dorsal side, P; palmar side, total carpal area (TCA, solid line), bone area (BA, dashed line); carpal tunnel area (CTA, dotted line), carpal tunnel depth (CTD, dash-dot line with arrow heads), carpal tunnel width (CTW, solid line with arrow heads).

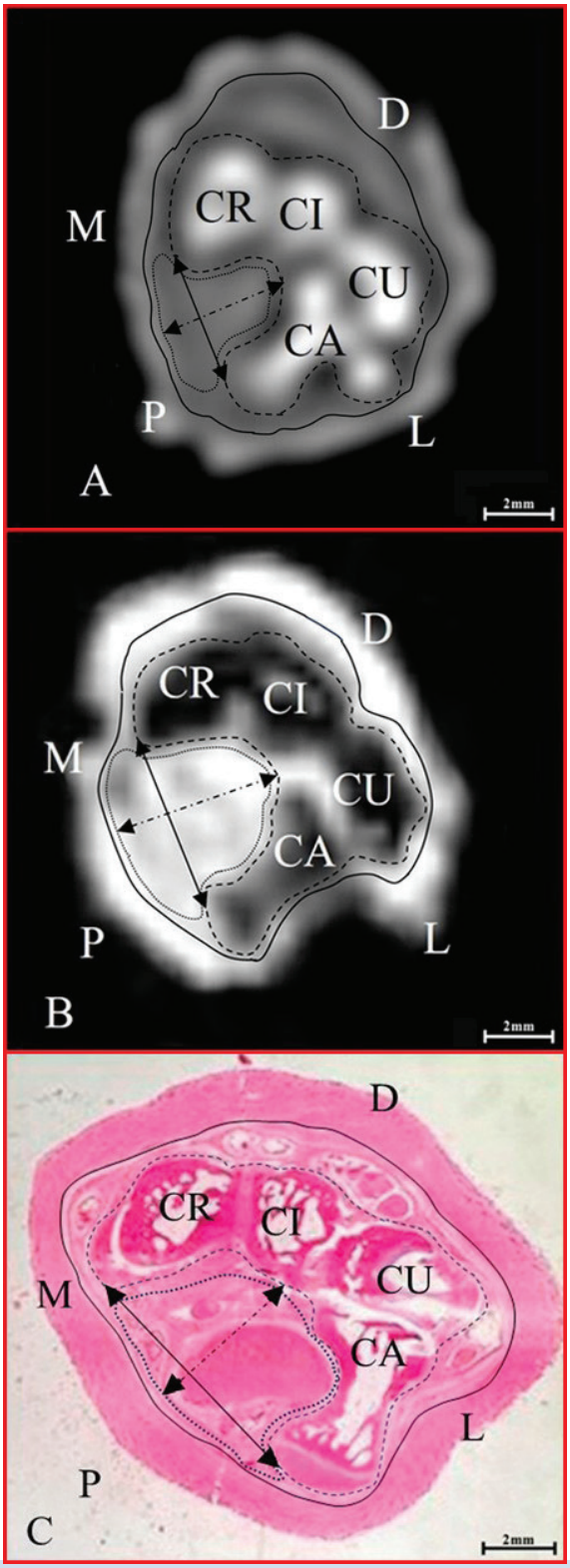

Figure 2. Images from computed tomography (bony window) (A), magnetic resonance (T1W) (B) and histological section (C) (H&E, 2X magnification) at the distal level. R; radius, U; ulna, CA; accessory carpal bone, M; medial side, L; lateral side, D; dorsal side, P; palmar side, total carpal area (TCA, solid line), bone area (BA, dashed line); carpal tunnel area (CTA, dotted line), carpal tunnel depth (CTD, dash-dot line with arrow heads), carpal tunnel width (CTW, solid line with arrow heads).

using CT, MRI and histological methods. CT images obtained from the bony window were evaluated. The structure of the carpal tunnel was clearly seen on the T1W transverse images obtained from a 3 Tesla MRI. Histological sections and anatomical dissections permitted easy identification of soft tissue and bones.

On CT and MR images (Figure 1), the top of the carpal tunnel showed the ends of the radius and ulna, as well as the palmar projection of the accessory carpal bone (pisiform). At the end of CT and MR images (Figure 2), the proximal row of carpal bones, including the radial carpal (scaphoid), intermediate carpal (lunate), ulnar carpal (triquetrum), and accessory carpal bones (pisiform) were defined. Because the carpal regions in rabbits were tiny, the soft tissues at both levels could not be identified in CT and MRI. Therefore, the soft tissues were defined with histological sections and anatomical dissection guidance.

It was observed that the flexor retinaculum bound the carpal tunnel on the palmar side. It was attached laterally to the palmar projection of the accessory carpal bone. Medially, it is connected to the edges of the radius, radial carpal and primum carpal (trapezium) bones. The flexor retinaculum consisted of two layers as named superficial and deep. These two layers were connected in the middle part of the flexor retinaculum, but they were divided on the lateral and medial sides where they attached (Figure 3). The deep digital flexor tendon, superficial digital flexor tendon and radial carpal flexor tendon are observed within the carpal tunnel. It was determined that the deep digital flexor tendon was located dorsal to the superficial digital flexor tendon and on the medial side of the accessory carpal bone. The superficial digital flexor was in the form of a three-piece tendon, while the deep digital flexor was a single large tendon. The radial carpal flexor tendon was found on the dorsomedial side of the deep digital flexor tendon. It was located on the palmar side of the radius at the proximal level and on the palmar side of the radial carpal bone at the distal level (Figure 4 & 5).

There was a bundle of connective tissue sheath surrounding the median nerve, median artery, caudal interosseus artery, median vein, and caudal interosseus vein. This vascular nerve bundle was observed medially to the deep digital flexor tendon and the radial carpal flexor tendon. This structure was located on the palmomedial side of the radius at the proximal level and on the radial carpal bone at the distal level. There was a bundle of connective tissue sheath surrounding

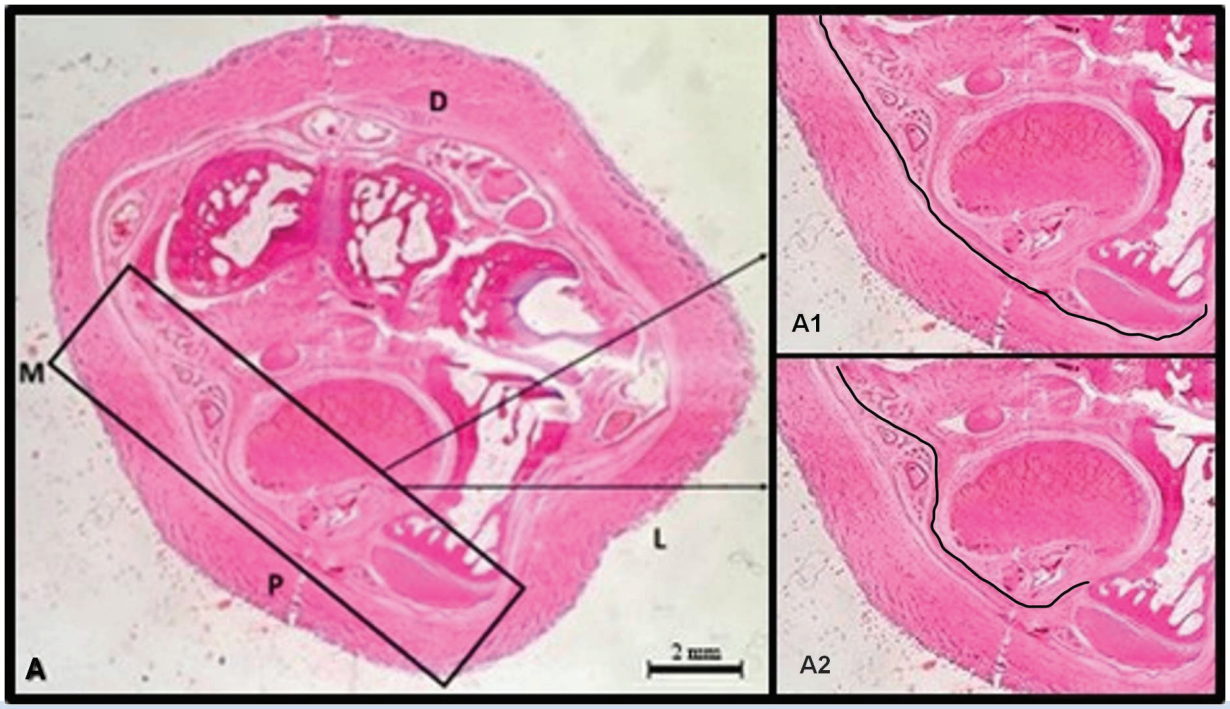

Figure 3. Image from histological section at the carpal tunnel (distal level) (H&E, 2X magnification) and representation of the flexor retinaculum's layers. (A). A1; flexor retinaculum superficialis, A2; flexor retinaculum profundus, M; medial side, L; lateral side, D; dorsal side, P; palmar side.

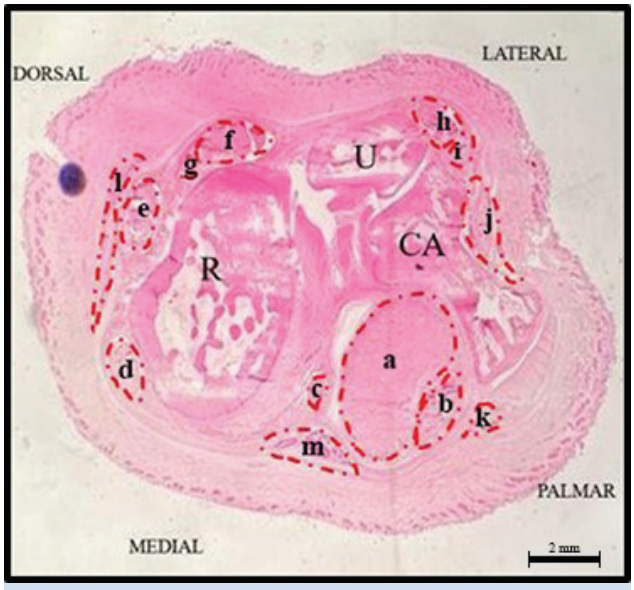

Figure 4. Image from histological section at the carpal tunnel entrance (proximal level) (H&E, 2X magnification). R: radius, U: ulna, CA: accessory carpal bone, a; deep digital flexor tendon, b; superficial digital flexor tendon, c; radial carpal flexor tendon, d; abductor pollicis longus tendon, e; radial carpal extensor tendon, f; common digital extensor tendon, g; primum and secundum digital extensor tendon, h; ulnar carpal extensor tendon, i; lateral digital extensor tendon, j; vascular nerve bundle (dorsal ramus of ulnar nerve, ulnar artery and ulnar vein), k; palmar ramus of ulnar nerve, l: vascular nerve bundle (radial artery, accessory cephalic vein and radial nerve), m; median nerve bundle (median nerve, median artery, caudal interosseus artery, median vein and caudal interosseus vein).

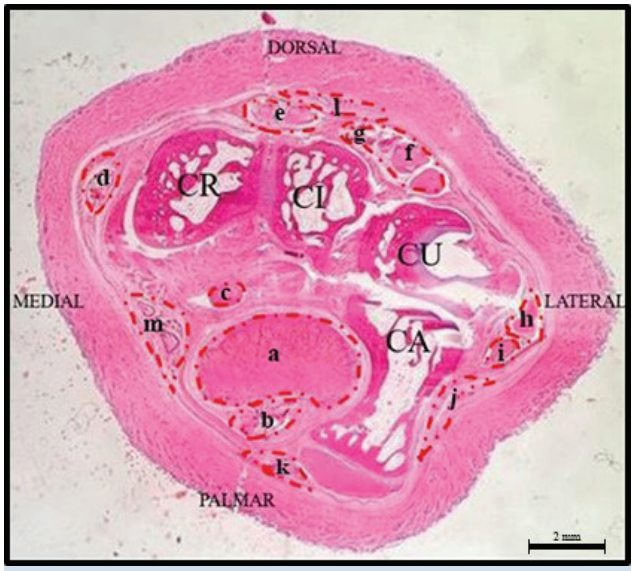

Figure 5. Image from histological section at the carpal tunnel (distal level) (H&E, 2X magnification). CR: radial carpal bone, CI: intermediate carpal bone, CU: ulnar carpal bone, CA: accessory carpal bone, a; deep digital flexor tendon, b; superficial digital flexor tendon, c; radial carpal flexor tendon, d; abductor pollicis longus tendon, e; radial carpal extensor tendon, f; common digital extensor tendon, g; primum and secundum digital extensor tendon, h; ulnar carpal extensor tendon, i; lateral digital extensor tendon, j; vascular nerve bundle (dorsal ramus of ulnar nerve, ulnar artery and ulnar vein), k; palmar ramus of ulnar nerve, l: vascular nerve bundle (radial artery, accessory cephalic vein and radial nerve), m; median nerve bundle (median nerve, median artery, caudal interosseus artery, median vein and caudal interosseus vein).

the ramus palmaris of the ulnar nerve, which included the arteriole and venule. The bundle was located on the palmolateral side of the superficial digital flexor tendons and the palmomedial side of the accessory carpal bone at these two levels. Both bundles were taken part within two layers of the flexor retinaculum and passed through the carpal tunnel (Figure 4 &5).

When the measurements between the proximal and distal levels were compared, decreases were obtained in the total carpal area, carpal tunnel area, and bone area at the distal level by three visualization methods. In CT and MRI data, the decrease in total carpal area was found to be statistically significant (P= 0.044, P= 0.022, respectively), while in histological data, the decrease in bone area was found to be statistically significant (P= 0.001) (Table 1 & 2). Furthermore, at both levels, the ratio of carpal tunnel area to total carpal area was calculated. As a result, the ratios in CT and MR images were seen to be close to each other, even though there was a decrease in histological sections at the transition to the carpal tunnel (Figure 6).

Regarding to CTW measurement towards the distal level, an increase in CTW was seen in computer tomography and magnetic resonance images but a decrease in histological section images. The condition is reversed in CTD measurements. Furthermore, the decrease in CTD data in computer tomography was found to be statistically significant (P= 0.015) (Table 2).

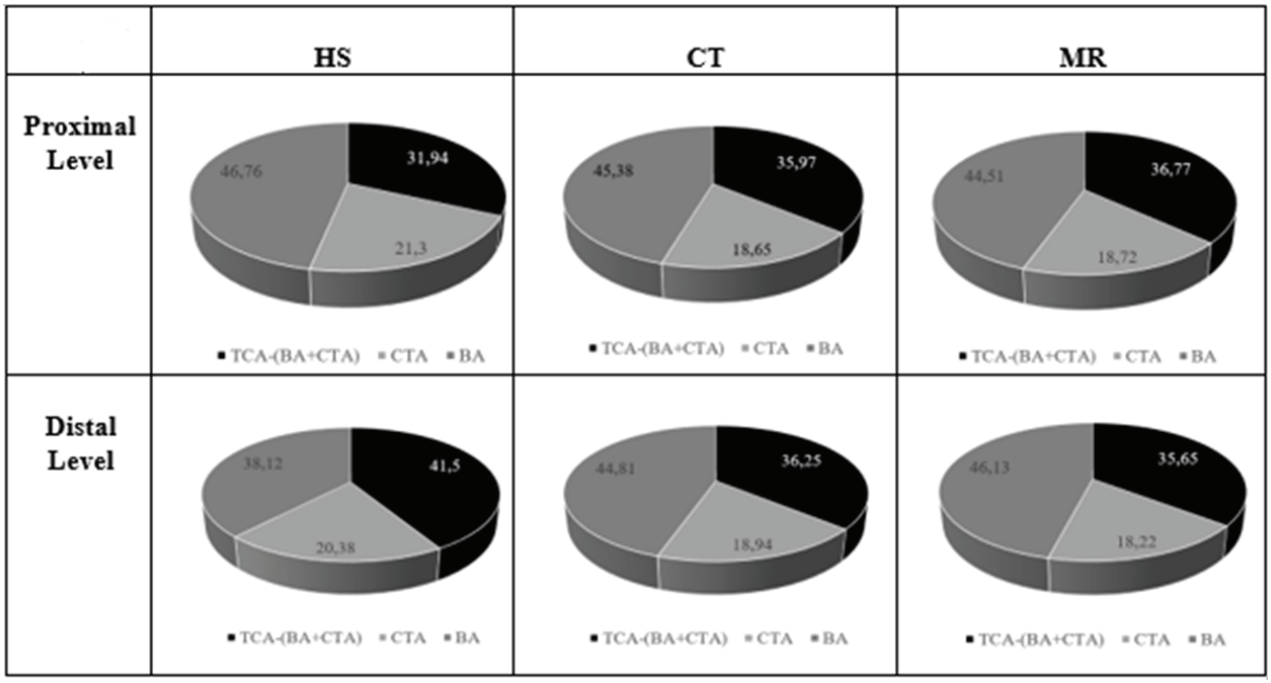

Figure 6. The ratios of carpal tunnel area and bone area to total carpal area in the histological (HS). computed tomography (CT) and magnetic resonance imaging (MRI) sections. CTA; carpal tunnel area, TCA; total carpal area, BA; bone area.

Table 1. The measurements at the proximal and distal levels of the carpal region by histological sections (HS), computed tomography (CT), and magnetic resonance imaging (MRI). TCA; total carpal tunnel area, CTA; carpal tunnel area, BA; bone area, CTW; carpal tunnel width, CTD; carpal tunnel depth, CAL; accessory carpal bone length.

		HS		CT		MRI	
		Proximal level	Distal level	Proximal level	Distal level	Proximal level	Distal level
	n	Mean±Std	Mean±Std	Mean±Std	Mean±Std	Mean±Std	Mean±Std
TCA (mm^2)	8	86.10±2.89	85.85±3.19	104.66±3.45	100.77±4.61	107.24±3.11	102.56±3.09
CTA (mm^2)	8	18.34±1.14	17.50±0.49	19.52±1.39	19.09±0.94	20.07±1.71	18.69±1.22
BA (mm^2)	8	40.26±3.40	32.73±1.15	47.49±1.70	45.15±3.23	47.73±4.85	47.31±2.77
CTW (mm)	8	5.96±0.44	5.84±0.20	4.91±0.32	4.98±0.37	4.97±0.33	5.15±0.53
CTD (mm)	8	3.98±0.26	4.04±0.16	4.42±0.25	4.35±0.32	4.62±0.31	4.55±0.55
CAL (mm)	8		4.50±0.81		4.73±0.41		4.62±0.29

Table 2. Comparison of data by histological sections. CT and MRI at the proximal and distal levels of the carpal region using paired statistical analysis.

	Proximal Level					Distal Level				
	TCA	**BA**	**CTA**	**CTW**	**CTD**	**TCA**	**BA**	**CTA**	**CTW**	**CTD**
HS-CT	0.000	0.003	0.010	0.000	0.004	0.000	0.000	0.005	0.002	0.042
HS-MRI	0.000	0.003	0.004	0.002	0.001	0.000	0.000	0.027	0.020	0.028
CT-MRI	NS	NS	NS	NS	NS	NS	NS	NS	NS	NS

NS: Not Significant

When the measurements from three methods were compared in pairs, it was found that the MRI and CT data were similar, but the histological method data were lower than the data obtained from MRI and CT at both levels, except for CTW. When data from the histological sections was compared to data from other methods, the differences were statistically significant (Table 1).

The accessory carpal bone was completely visualized at the distal level. The histological section's measurement of the accessory carpal bone's length was shorter than the measurements made using the other techniques (Table 1). The accessory carpal bone constitutes the palmolateral border of the carpal tunnel and defines the carpal tunnel depth. Therefore, the ratio between carpal tunnel depth and accessory carpal bone length was evaluated. It was determined that CAL/CTD: 1.15 in histological method, 1.09 in CT, and 1.07 in MRI.

DISCUSSION

The carpal tunnel is bordered by the hole between the carpal bones and the flexor retinaculum. Because of structural variances, the borders of the carpal tunnel vary between species. The bone roof of the carpal tunnel in rabbits is similar to that in dogs. Therefore, the carpal tunnel was investigated as entrance and exit at two levels in this study, as in dogs.

The palmary boundary of the carpal tunnel is the flexor retinaculum, also known as the transverse carpal ligament, which has been reported to exist in two layers in humans (Presazzi *et al.,* 2011). The median nerve, four deep digital flexor tendons, four superficial digital flexor tendons and a flexor pollicis longus tendon pass through this tunnel. On its medial side, the flexor retinaculum splits into two layers to envelop the radial carpal flexor tendon. On its lateral side, the ulnar nerve travels through the tunnel known as Guyon's canal (Presazzi *et al.,* 2011; Deak *et al.,* 2022). In dogs, the flexor retinaculum has been reported to also consist of two layers. However, in contrast to humans, the superficial digital flexor tendon is situated between these two layers. The radial carpal flexor tendon, median nerve, ulnar nerve, caudal interosseous arteries and caudal interosseous veins are located with the deep digital flexor tendon under the profound layer of the flexor retinaculum in the carpal tunnel (Turan and Erden, 2003). Detailed morphological information of the flexor retinaculum was not found in previous studies in rabbits (Ettema *et al.,* 2006; Schrier *et al.,* 2020). In this study, it was determined that the flexor retinaculum in rabbits has two layers. It was observed that the median nerve bundle and the ulnar nerve bundle were located between these two layers at the medial and lateral tips of the retinaculum flexorum. In addition, the structures in these vascular nerve bundles have not been mentioned in detail (Ettema *et al.,* 2006; Ekim *et al.,* 2014; Schrier *et al.,* 2020). We observed that the median nerve, median artery, caudal interosseus artery, median vein, and caudal interosseus vein were included in the median vessel nerve bundle. In this study, the ramus palmaris of the ulnar nerve, arteriole and venule were found in the ulnar nerve package. It should be noted that there is a radial carpal flexor tendon but no flexor pollicis longus tendon in the carpal tunnel in rabbits, which does not agree with the previous studies (Ettema *et al.,* 2006; Ekim *et al.,* 2014; Schrier *et al.,* 2020).

Carpal tunnel area is an important criterion in the evaluation of carpal tunnel syndrome and varies in people according to variables such as race and gender. Rodríguez *et al.* (2022) reported the carpal tunnel area in humans as 188.00 ± 33.8 mm^2 in men and 144.3 ± 19.5 mm^2 in women using cadaver sections. Kamolz *et al*. (2001) compared the carpal tunnel area in humans using ultrasound and anatomical sections and found it to be 162.4 ± 29.3 mm^2 and 168.2 ± 31.2 mm^2, respectively. Furthermore, the carpal tunnel area in humans has been measured at the neutral position by MRI to be 173-178 mm^2 at the proximal level and 152-158 mm^2 at the distal level (Horch *et al.,* 1997;

Yoshioka *et al.,* 1993). Turan and Erden (2003) measured the carpal tunnel area with CT in German Wolfhound dogs and reported the average (proximal and distal) carpal tunnel area delimited by the profound layer to be 156.93 ± 14.5 mm^2 in males and 131.99 ± 9.08 mm^2 in females. It has also been reported that the carpal tunnel area bounded by the superficial layer is approximately 1.70 times (in males) and 1.84 times (in females) that of the profound carpal tunnel. In this study, the mean proximal and distal levels of the carpal tunnel areas were determined as 17.92 ± 0.82 mm^2 in histological sections, 19.31 ± 1.17 mm^2 in CT, and 19.38 ± 1.47 mm^2 in MRI in rabbits. The carpal tunnel area of rabbits was seen to be approximately 1/8-9 that of humans in CT and MR images, while it was 1/9 in histological sections. In dogs, this rate was changed. Take the boundary of the profound layer of the flexor retinaculum, the carpal tunnel area of rabbits was seen to be approximately 1/7 that of dogs, and the superficial layer boundary of it was 1/13 that of dogs in CT.

The dimensions (depth and width) of the carpal tunnel in human cadavers were measured in a silicone cast and have been reported to be 8.3 ± 0.9 mm and 19.2 ± 1.7 mm, respectively (Pacek *et al.,* 2010). Using ultrasound and anatomical sections in humans, it has been found that the depth is 9.0 ± 1.1 mm with a width of 20.5 ± 1.5 mm and 9.3 ± 1.2 mm depth and 20.1 ± 1.5 mm width, respectively (Kamolz *et* al., 2001). Mogk and Keir (2008) have reported the depth and width of the carpal tunnel as 10.7 mm and 22.5 mm at the proximal level and 10.6 mm and 21.5 mm at the distal level in humans by MRI, respectively. Turan and Erden (2003) used CT to measure the depth and width of the carpal tunnel in dogs, noting that the depth was 16.99 mm at the proximal and 19.53 mm at the distal level, while the width was 15.50 mm at the proximal and 17.73 mm at the distal level. According to our findings in this study, it was determined that the width of the carpal tunnel in rabbits was approximately one-quarter that of humans and one-third that of dogs, and its depth was approximately half that of humans and one-fourth that of dogs. The width is greater than the depth in rabbits, similar to humans, whereas this is the opposite in dogs. In this study, the width of the carpal tunnel increased from proximal to distal and the depth decreased, while the opposite was seen in dogs. The carpal tunnel shape is oval in humans, isosceles triangular in dogs, and close to round in rabbits. These alterations in shape are presumed to be caused by the hook of os carpale IV (hamate) and the species being digitigrade or plantigrade.

Studies on the carpal tunnel in humans have found that the carpal tunnel is narrower at the distal level due to the hook of os carpale IV (hamate) is located there (Yoshioka *et al.,* 1993; Horch *et al.,* 1997; Sora and Genser-Strobl, 2005). Turan and Erden (2003) investigated the ratio of carpal tunnel to total carpal area using CT in dogs and reported that the carpal tunnel forms 18-19 % of the total carpal area at the proximal level and 19-22 % at the distal level. They suggested that the carpal tunnel area in the distal cross-section is wider than that in the proximal section. In the present study, the ratios were found to be similar at both levels in CT and MRI cross-sections. In histological sections, this ratio was seen to have slightly decreased towards the distal level. This difference is believed to be due to the decalcification process used in the histological method.

Imaging methods have advantages and disadvantages. Bone tissue images are clearer and more accurate in CT images and soft tissue images in MR images (Vogl et al. 2010; Derudere et al. 2014). Histological section images are the most advantageous in terms of imaging two different tissues. The very small size of the carpal tunnel in rabbits has caused limitations in MRI and CT imaging methods. Although the small digital channel coil was used in MR imaging methods, there were difficulties in obtaining the desired soft tissue data. For this reason, the histological section method and anatomical dissection were very useful in examining the region. However, fixation and decalcification processes applied in histological methods cause shrinkage in tissues (Tagi et al., 2018). By evaluating the advantages of these methods, we compared all three images, determined reference points, and measured them in this study.

CONCLUSIONS

In this study, the carpal tunnel anatomy of rabbits was examined in detail with different methods and we attempted to clarify the insufficient and inaccurate data in earlier studies of carpal tunnel syndrome in rabbits. The main findings of this study significantly emphasize the validation of the rabbit model in carpal tunnel syndrome research. By establishing the closer resemblance of the rabbit carpal canal to humans compared to dogs, this research paves the way for more accurate investigations into the condition. The utilization of the rabbit model holds the potential to enhance our understanding of carpal tunnel syndrome

and improve treatment strategies for human patients, ultimately leading to better clinical outcomes.

ACKNOWLEDGMENTS

This study was derived from the PhD thesis of the first author. This research has been supported within the content of the project no VTF-19025 by Aydin Adnan Menderes University

CONFLICT OF INTERESTS

The authors declared that there is no conflict of interest.

REFERENCES

Bower JA, Stanisz GJ, Keir PJ (2006) An MRI evaluation of carpal tunnel dimensions in healthy wrists: Implications for carpal tunnel syndrome. Clin Biomech, 21: 816-825.

Craige EH (1948) Practical Anatomy of the Rabbit. (5th ed.), The Blakiston Company, Philadephia,

Deak N, Black AC, Bordoni B (2022) Anatomy, Shoulder and Upper Limb, Wrist Flexor Retinaculum. In StatPearls. StatPearls Publishing.

Deruddere KJ, Milne ME, Wilson KM, Snelling SR (2014) Magnetic resonance imaging, computed tomography, and gross anatomy of the canine tarsus. Vet Surg, 43: 912-919.

Diao E, Shao F, Liebenberg E, Rempel D, Lotz JC (2005). Carpal tunnel pressure alters median nerve function in a dose-dependent manner: a rabbit model for carpal tunnel syndrome. J. Orthop. Res., 23: 218-223.

Ekim O, Oto Ç, Algın O (2014) Magnetic Resonance (MR) Imaging of The Carpal Tunnel and Related Structures In New Zealand Rabbit (Oryctolagus Cuniculus): An Anatomic and Radiologic Evaluation On An Animal Model. Vet J Ankara Univ, 61:1-7.

Ettema AM, Zhao C, An KN, Amadio PC (2006) Comparative anatomy of the subsynovial connective tissue in the carpal tunnel of the rat, rabbit, dog, baboon, and human. Hand, 1: 78-84.

Horch R, Allmann KH, Laubenberger J, Langer M, Stark GB (1997) Median nerve compression can be detected by magnetic resonance imaging of the carpal tunnel. Neurosurgery 41: 76- 82

Kamolz LP, Schrögendorfer KF, Rab M, Girsch W, Grube, H, Frey M (2001) The precision of ultrasound imaging and its relevance for carpal tunnel syndrome. Surg Radiol Anat, 23: 117-121.

Luna, LG (1968) Manual of histologic staining methods of the Armed Forces Institute of Pathology. 3rd Edition, McGraw-Hill, New York.

Mogk JP and Keir PJ (2008) Wrist and carpal tunnel size and shape measurements: effects of posture. Clin Biomech, 23: 1112-1120.

Moriya T, Zhao C, Cha SS Schmelzer JD, Low PA, An KN, Amadio PC (2011) Tendon injury produces changes in SSCT and nerve physiology similar to carpal tunnel syndrome in an in vivo rabbit model. Hand, 6: 399-407.

Ng AWH, Griffith JF, Tong CSL, Law EKC, Tse WL, Wong CWY, Ho PC (2020) MRI criteria for diagnosis and predicting severity of carpal tunnel syndrome. Skeletal Radiol, 49: 397- 405.

Oh S, Ettema AM, Zhao C, Zobitz ME, Wold LE, An KN, Amadio PC (2008) Dextrose-induced subsynovial connective tissue fibrosis in the rabbit carpal tunnel: A potential model to study carpal tunnel syndrome? Hand, 3: 34-40.

Pacek CA, Tang J, Goitz RJ, Kaufmann RA, Li ZM (2010) Morphological analysis of the carpal tunnel. Hand, 5: 77-81.

Park JS, Won HC, Oh JY, Kim DH, Hwang SC, Yoo JI (2020) Value of cross-sectional area of median nerve by MRI in carpal tunnel syndrome. Asian J Surg, 43: 654-659.

Presazzi A, Bortolotto C, Zacchino M, Madonia L, Draghi F (2011) Carpal tunnel: Normal anatomy, anatomical variants and ultrasound technique. J Ultrasound, 14: 40-46.

Rodríguez P, Casado A, Potau JM (2022) Quantitative anatomical analysis of the carpal tunnel in women and men. Ann Anat, 243: 151956.

Schrier VJMM, Vrieze A, Amadio PC (2020) Subsynovial connective tissue development in the rabbit carpal tunnel. Vet Med Sci, 6: 1025-1033.

Sora MC and Genser-Strobl B (2005) The sectional anatomy of the carpal tunnel and its related neurovascular structures studied by using plastination. Eur J Neurol, 12: 380-384.

Stapleton MJ (2006) Occupation and carpal tunnel syndrome. ANZ J Surg, 76: 494-496.

Taqi SA, Sami SA, Sami LB, Zaki SA (2018). A review of artifacts in histopathology. JOMFP, 22: 279.

Tung WL, Zhao C, Yoshii Y, Su FC, An KN, Amadio PC (2010) Comparative study of carpal tunnel compliance in the human, dog, rabbit, and

rat. J Orthop Res, 28: 652-656.
Turan E and Erden H (2003) Computed tomography and morphometry of the carpal canal in the dog. Ann Anat, 185: 173-178.
Vogl TJ, Harth M, Siebenhandl P (2010). Different imaging techniques in the head and neck: Assets and drawbacks. World J Radiol, 2: 224-229.
Wright AR and Atkinson RE (2019) Carpal Tunnel Syndrome: An Update for the Primary Care Physician. Hawai'i J Health Soc Welf, 78: 6-10.
Yamaguchi T, Osamura N, Zhao C, Zobitz ME, An KN, Amadio PC (2008) The mechanical properties of the rabbit carpal tunnel subsynovial connective tissue. J Biomech, 41: 3519- 3522.
Yoshii Y, Zhao C, Schmelzer JD, Low PA, An KN, Amadio PC (2014) Effects of multiple injections of hypertonic dextrose in the rabbit carpal tunnel: a potential model of carpal tunnel syndrome development. Hand, 9: 52-57.
Yoshioka S, Okuda Y, Tamai K, Hirasawa Y, Koda Y (1993) Changes in carpal tunnel shape during wrist joint motion - MRI evaluation of normal volunteers. J Hand Surg, 18B: 620- 623.
Zuniga AF and Keir PJ (2019) Diagnostic and Research Techniques in Carpal Tunnel Syndrome. Crit Rev Biomed Eng, 47: 457-471.